Statistical learning for complex data to enable precision medicine strategies

Zwep, L.B.

Chapter 3

Identification of high-dimensional omics-derived predictors for tumor growth dynamics using machine learning and pharmacometric modeling

Authors

Laura B. Zwep

Kevin L. W. Duisters

Martijn Jansen

Tingjie Guo

Jacqueline J. Meulman

Parth J. Upadhyay

J. G. Coen van Hasselt

CPT: Pharmacometrics & Systems Pharmacology 2021; 10(4), 350–361

Abstract

Pharmacometric modeling can capture tumor growth inhibition (TGI) dynamics and variability. These approaches do not usually consider covariates in high-dimensional settings, whereas high-dimensional molecular profiling technologies ("omics") are being increasingly considered for prediction of anticancer drug treatment response. Machine learning (ML) approaches have been applied to identify high-dimensional omics predictors for treatment outcome. Here, we aimed to combine TGI modeling and ML approaches for two distinct aims: omics-based prediction of tumor growth profiles and identification of pathways associated with treatment response and resistance. We propose a two-step approach combining ML using least absolute shrinkage and selection operator (lasso) regression with pharmacometric modeling. We demonstrate our workflow using a previously published dataset consisting of 4706 tumor growth profiles of patient-derived xenograft (PDX) models treated with a variety of mono- and combination regimens. Pharmacometric TGI models were fit to the tumor growth profiles. The obtained empirical Bayes estimates-derived TGI parameter values were regressed using the lasso on high-dimensional genomic copy number variation data, which contained over 20,000 variables. The predictive model was able to decrease median prediction error by 4% as compared with a model without any genomic information. A total of 74 pathways were identified as related to treatment response or resistance development by lasso, of which part was verified by literature. In conclusion, we demonstrate how the combined use of ML and pharmacometric modeling can be used to gain pharmacological understanding in genomic factors driving variation in treatment response.

3.1 Introduction

Pharmacometric modeling of tumor growth inhibition (TGI) dynamics is extensively used to model the longitudinal response of tumor size in response to drug treatment in preclinical animal models or patients. Pharmacometric TGI models have increasingly been used to characterize drug-exposure response relationships using semi-mechanistic parameters related to, for instance, direct treatment effects or resistance to personalize drug treatment (Ribba et al., 2014; Bender et al., 2014). Using TGI models, interindividual variation in tumor growth rate, treatment efficacy, and treatment resistance can be quantified and related to patient-specific characteristics (Ribba et al., 2014; Rodriguez-Brenes et al., 2013). In recent years, TGI models have been integrated with time-to-event models to predict clinical outcomes, such as overall survival, which allow prediction of clinical outcomes based on the patient-specific tumor growth dynamics parameters (Claret et al., 2009; van Hasselt et al., 2015b, 2015a).

The use of high-dimensional molecular profiling technologies, including next-generation sequencing, to develop personalized treatment schedules is rapidly developing. In particular in oncology, the use of "omics" technologies to characterize tumor-

specific molecular differences to predict variation in treatment response is of great interest (Shlien & Malkin, 2009). Although both omics and TGI modeling are of relevance toward personalized treatment strategies, pharmacometric TGI models are not frequently directly applied to high-dimensional covariates. In pharmacometric modeling, stepwise covariate inclusion approaches are still the most commonly used approach to include covariates, which is unsuitable for testing of covariates in a high-dimensional setting.

Current analyses of high-dimensional "omics" datasets predicting treatment response are mostly performed using machine learning (ML) methodologies, such as sparse regression models, random forests, and deep learning, to obtain predictive signatures of treatment response (Degenhardt et al., 2017; Nicolò et al., 2020; Xie et al., 2019). The majority of studies with ML approaches are based on either dichotomous survival response or clinical response metrics, such as based on the Response Evaluation Criteria in Solid Tumors (RECIST) system (Lathrop & Kaklamani, 2018; Eisenhauer et al., 2009), wherein the observed dynamic tumor disease progression profile is reduced into a limited number of categories. These simplified categorical treatment response metrics lack biological or pharmacological relevance, because factors, such as resistance and direct treatment effects, are merged (Chadeau-Hyam et al., 2013).

A commonly used ML method is the least absolute shrinkage and selection operator (lasso), which is a linear regression method with ℓ_1 regularization that can be used for high-dimensional analysis, and results in variable selection (Tibshirani, 1996). Although ML approaches, such as sparse regression models using the lasso (Bertrand et al., 2008, 2015; Ribbing et al., 2007; Haem et al., 2017), have been implemented in pharmacometric modeling, they are computationally expensive due to the combination of nonlinearity and estimation of random effects, which often lead to convergence problems. The implementations of the lasso involve alternating algorithms, which alternate between estimating the random effects and the lasso optimization, so although lasso is rather efficient, iterating through multiple random effect estimation steps can severely reduce computational efficiency. This can lead to long computation times and poor convergence rates, especially in high-dimensional settings.

In this study, we propose a two-step approach combining ML, using lasso regression, with pharmacometric modeling. We demonstrate our approach using a large dataset consisting of longitudinal tumor growth profiles of patient-derived xenograft (PDX) models treated with a variety of mono- and combination regimens (Gao et al., 2015). We develop pharmacometric tumor growth models quantifying intertumor variation in growth rates, drug effect, and resistance, after which we implement ML-based lasso models to address the following aims: (1) to predict longitudinal tumor growth profiles based on omics-derived predictors using a multivariate lasso model; and (2) to identify biological pathways associated with interindividual variation in treatment response or resistance development using a group lasso regression model (Figure 3.1).

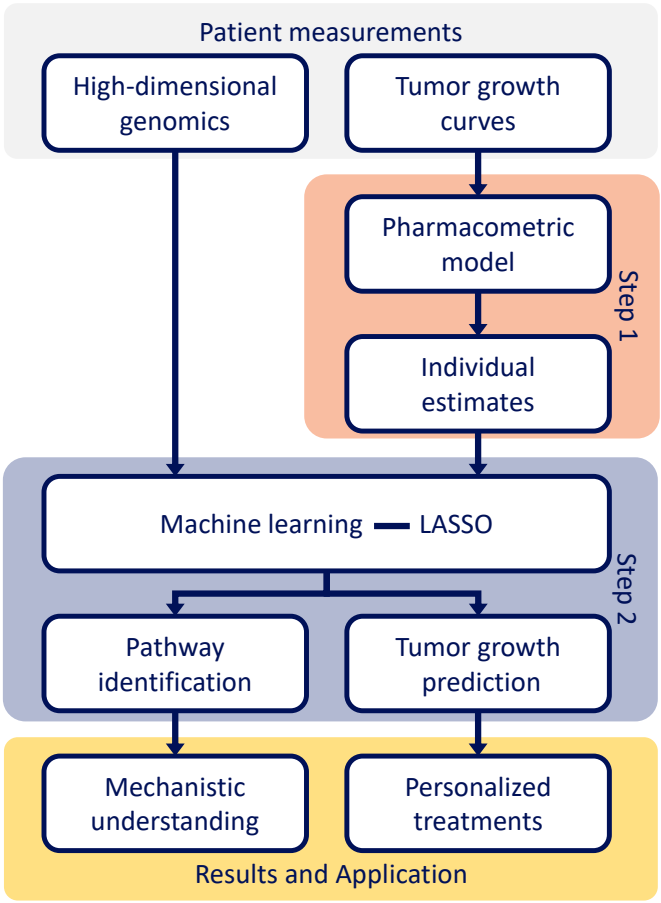

Figure 3.1: A schematic visualization of the proposed two-step approach. First, the tumor growth curves were modeled to obtain tumor growth parameter estimates, second, the individual estimates tumor growth parameter estimates were regressed on copy number variations (genomics) by different least absolute shrinkage and selection operator (lasso) techniques. The group lasso was applied to obtain biological pathways. The multivariate lasso was applied to predict the tumor growth parameter values, which were then inserted into the tumor growth inhibition model equations to obtain predictions of the tumor growth curves.

3.2 Methods

3.2.1 Data

Data from a large scale preclinical study in PDX mice models were used (Gao et al., 2015). This dataset consisted of over 4000 PDX experiments, which were derived from a total of 277 patients, where multiple PDX experiments were derived from the same tumor. The PDX experiments from one tumor were all treated with different anticancer agents as mono treatment or combination treatment, or left untreated (e.g., natural growth experiments). There was a total of 62 unique treatments and for every

tumor treated one PDX was left untreated, leading to an incomplete design with multiple PDX experiments per treatment. Tumor volume was measured daily. For each unique tumor, at the start of the treatment, genomic data based on gene copy number variations (CNVs) were obtained, yielding a total of 23,852 CNVs. We included data for 174 unique tumors and 55 unique treatments, corresponding with 3244 tumor-treatment combinations. This selection was based on availability of CNV data and adequate fit (see section below). The analysis was conducted separately for every treatment, so the number of observations differed per analysis, ranging from 17 to 171 observations (Table S3.1).

3.2.2 Tumor growth inhibition model

A TGI model was fitted to the longitudinal tumor volume measurements using the non-linear regression modeling software NONMEM (Beal & Sheiner, 1980), with first order conditional estimation with interaction(Claret et al., 2009). The TGI model captured the longitudinal tumor volume measurements, per PDX, through estimation of three parameters: growth rate (k_g), treatment efficacy (k_d), and time-dependent resistance development (k_r) in an ordinary differential equation (Equation 3.1).

$$\frac{dV_i(t)}{dt} = k_{g,i} \cdot V_i(t) - k_{d,i} \cdot e^{-k_{r,i} \cdot t} \cdot V_i(t) \tag{3.1}$$

with tumor volume $V(t)$ at time t and tumor growth model parameters k_g, k_d and k_r. Random effects with a log-normal distribution, were added to all fixed effect TGI parameters as following: $k_{g,i} = k_g \cdot exp\ (\eta_{k_g i})$.

To fit the TGI model, we first estimated individual value for k_g separately for every tumor using the untreated PDX data (Equation 3.2).

$$\frac{dV_i(t)}{dt} = k_{g,i} \times V_i(t) \tag{3.2}$$

The empirical Bayes estimates (EBEs) of k_g were extracted and included as data in the TGI model. EBEs in NONMEM is the estimation of the posterior individual random effects ($\hat{\eta}_i$), based on the empirically obtained prior distribution of η and the individual data, as previously described (Sheiner et al., 1972). The residual error was modeled with both an additive and proportional error.

We observed that not all tumor growth curves showed time-dependent resistance development (e.g., regrowth), so both a full TGI model and a reduced model, without a term for resistance, were fitted, effectively allowing k_r to become zero. For every PDX, a likelihood ratio test was conducted to evaluate whether inclusion of k_r added significantly to the model fit (at significance level 0.05). A second criterium was added to only select the full model if the k_r was estimated to be smaller than 1.0, because the term $k_d \cdot e^{k_r \cdot t}$ goes to zero very fast with t for larger k_r, effectively making k_d unidentifiable.

To evaluate the model fit separately for each treatment, we plotted the conditional weighted residuals per treatment, which represent the goodness of fit for the TGI

models (Nguyen et al., 2017). Due to the large number of tumor growth curves, treatments with curves with a bad model fit were removed from further analysis. The EBEs of k_d and k_r were extracted for the treatments with good model fit.

3.2.3 Tumor growth profile prediction

The multivariate outcome the log-transformed k_g, log-transformed k_d, and k_r was regressed on the genomic CNV data within every treatment using a multivariate lasso (Equation 3.3) (Simon et al., 2013). The multivariate lasso, similarly to the standard lasso, minimized the loss function to estimate the linear parameters β is mainly due to outcome Y and parameter β, which are, in this case, both matrices containing a column for every outcome. The penalty term is the root of the summed square error over the vector β_j.

$$\hat{\beta}_{MVlasso} = \arg\min_{\beta}(||Y - X\beta||_2^2 + \lambda \sum_{j=1}^{p} ||\beta_j||_2) \tag{3.3}$$

The lasso hyperparameter λ, which determines the size and number of non-zero parameters, was chosen through 10-fold cross-validation, to identify the λ which minimized the prediction error in terms of mean squared error. This minimizing λ differed per treatment. The treatments where the minimizing λ did not outperform the null model, which estimated no non-zero coefficients for the CNVs, were removed from further analysis, both in prediction of the tumor growth curves and the pathway selection. In a second analysis, only the log-transformed k_g, log-transformed k_d were regressed on the CNV data. Prediction errors were evaluated both on the scale of the predicted parameter values and on the scale of the predicted tumor growth curves.

The individual TGI parameter values predicted from the lasso were extracted. The ordinary differential equation (Equation 3.1 was solved for these predicted parameter values to bring the predictions back on the longitudinal tumor volume scale. For robustness, the cross-validation step was repeated twenty times over different cross-validation splits and the predicted curves were averaged over the twenty repetitions.

A measure of prediction error was defined on tumor curve scale through comparing the curves from the estimated parameters from the TGI model to the curves with the predicted parameters from lasso. The prediction error was defined as the absolute fraction of the area between the predicted and the estimated curves (ABC) over the area under the estimated curve (AUC), called the scaled ABC (sABC, Equation 3.4).

$$sABC_i(\tau) = \frac{\int_0^{\tau} |\tilde{V}_i(t) - \hat{V}_i(t)|dt}{\int_0^{\tau} \tilde{V}_i(t)dt} \tag{3.4}$$

for individual i with volume $\tilde{V}_i(t)$ estimated from the TGI model fit (IPRED) and volume $\hat{V}_i(t)$ predicted from the multivariate lasso. The area is considered until some cut-off τ, which in our study was set to 56 days (two months). The sABC was used because

it is a one-dimensional and interpretable error measure. The sABC metric allowed for the comparison of the two functions produced by the TGI model fit and the lasso parameter value prediction. The sABC of the lasso with CNVs was compared with the sABC of the null model, to see whether the CNVs added predictive power.

3.2.4 Pathway selection

To gain biological insight gained beyond selection of individual genes contributing to the predictive performance of treatment efficacy and time-dependent resistance development, the log-transformed k_d and k_r were separately regressed on the CNVs through pathway analysis using overlapping group lasso (Yuan & Lin, 2006; Jacob et al., 2009). The overlapping grouped lasso uses a combination of the lasso and the ℓ_2 norm, a square root of the sum of squares of the coefficients, which is also used for RIDGE regression (Hoerl & Kennard, 1970), to select variables on a group level (Equation 3.5). Each of the G groups contain a set of indices $\Im_g$, including all parameter indices of the β's in group g. The size of the group is denoted as $|\Im_g|$, which is used to scale the penalty to account for the different group sizes.

$$\hat{\beta}_{grouplasso} = \arg\min_{\beta}(||Y - X\beta||_2^2 + \lambda \sum_{g=1}^{G} \sqrt{|\Im_g|}||\beta_{\Im_g}||_2) \tag{3.5}$$

The groups were defined as the pathways from the WikiPathways ontology, which contains a comprehensive overview of biological pathways and processes (Kuleshov et al., 2016; Chen et al., 2013; Kutmon et al., 2015). A total of 5,998 CNVs was grouped to one or more pathways.

Again, ten-fold cross-validation was used to identify the λ, which determined how many pathways were selected. While utilizing a combination of ℓ_1 and ℓ_2 penalties, there is only one hyperparameter in the group lasso (Yuan & Lin, 2006). Subsequently, part of the discovered correlations between pathways and treatment response was researched in literature for validation. This analysis was conducted in R (R Core Team, 2020) (version 3.6.3) using the library grpregOverlap (`https://github.com/YaohuiZeng/grpregOverlap`).

3.2.5 Code availability

All scripts and models use for the analysis are available on github (`https://github.com/vanhasseltlab/PDX`).

3.3 Results

3.3.1 Tumor growth inhibition model development

The TGI model was fitted to the PDX tumor growth curves, separately for every treatment. For three treatments, no model was converged, these were left out of the anal-

ysis. The model fit was evaluated through the conditional weighted residuals (Figure S3.1) and the visual inspection of the PDX fits (Figure S3.2). The visual inspection showed the tumor dynamics for treatment TAS266 were not captured. Combination therapy LFW527 and binimetinib showed skewed residual distributions. The two treatments were discarded for further analysis. The model fit for the other treatments was sufficient.

All individual parameter estimates (EBEs) were extracted from the TGI model (Figure 3.2a). Figure 3.2b shows how the values of the parameter estimates affect the curve. The percentage of PDX experiments with non-zero time-dependent resistance development was 12.6%. The TGI model for the chosen treatments showed sufficient fits for the next step parameter values prediction step.

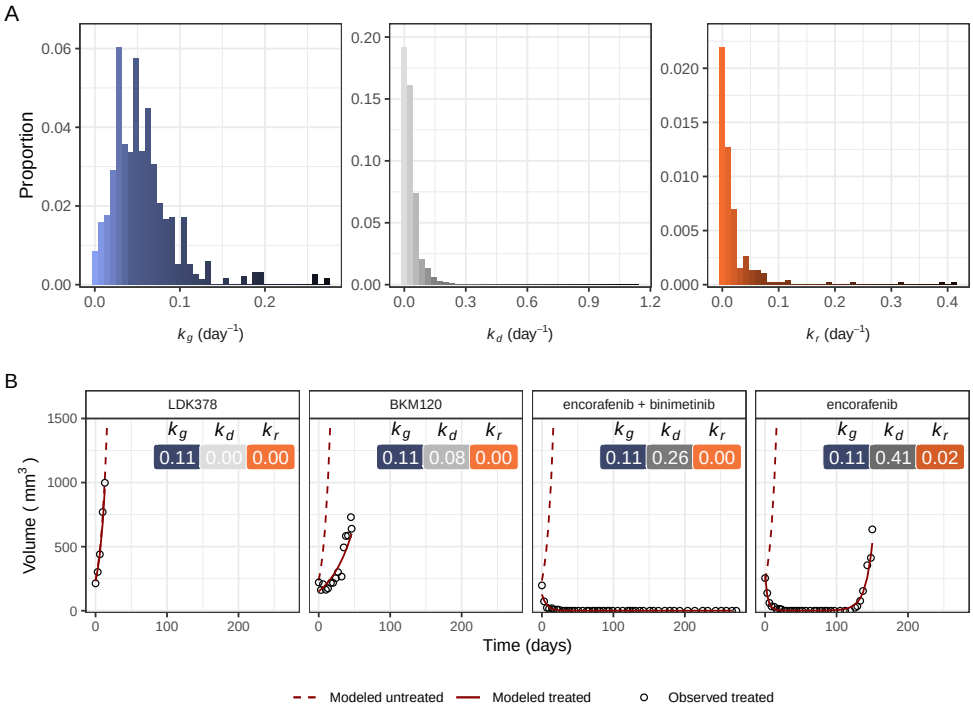

Figure 3.2: Results of the tumor growth inhibition (TGI) model estimation. A) The distributions of the individual, estimated TGI parameters. B) Selected tumor growth profiles showing how k_d and k_r vary for different treatments, with from left to right a very ineffective treatment, a slightly effective treatment, a very effective treatment and a very effective treatment with time-dependent resistance development.

The effect of shrinkage of the individual prediction values (η), often referred to as eta-shrinkage, was evaluated in Figure S3.2. The fit of the individual growth curves was not influenced by shrinkage. Since the tumor volumes were densely sampled over time, with an averages of 0.3 samples per day, 50 days follow-up time and 14 measurements per experiment, we did not expect problems with shrinkage.

3.3.2 Prediction of tumor growth profiles using genomic predictors

The estimated individual TGI parameters k_r, log-transformed k_d and log-transformed k_g were simultaneously predicted by the multivariate lasso. The prediction errors for the k_g, k_d and k_r were calculated as root mean square error. Although the variation between the treatments was high (Figure S3a), overall the RMSE was high. For k_g, the RMSE was 0.035, while a mean estimated k_g of 0.0564. For both the k_d and the k_r the RMSEs, 0.044 and 0.049 respectively, were actually higher than the mean estimated k_d (0.033) and the k_r (0.0564), indicating a bad prediction of the tumor growth dynamics from CNVs. A multivariate lasso with only the log-transformed k_d and log-transformed k_g was also fitted. These two lasso models were compared based on the prediction error of the log-transformed k_d and log-transformed k_g and the sABC error measure (Figure S3), where the model without predicting the k_r seemed to fit better, especially in the case of combination therapies BYL719 and cetuximab, and BKM120 and LJC049, which was used for consecutive analysis.

Out of 52 treatments, 33 treatments were detected with a better prediction than the null model, based on the average MSE over the cross-validation replications. For the other treatments, the predictive ability was not improved by adding CNVs as predictors to the lasso regression. The log k_g and log k_d were transformed back to their original scale and the parameters were used to solve the ordinary differential equation (Eq. 1) from the model.

The predictive performance of the lasso for predicting the TGI parameter values was evaluated by comparing the curves from the predicted estimates to the curves from the TGI model fit, since the estimated curves were already shown to fit the data well. The predictions and estimations are functions instead of measures, so the scaled area between the curves was calculated as error. The overall median sABC is 0.456, which can be interpreted as the area between the predicted and estimated curve, is less than half the area below the estimated curve (Figure 3.3a). The sABC distributions for the different treatments were shown (Figure 3.3b). A lower sABC shows a lower prediction error. 23.6% of the curves has an sABC below 0.2, so the difference between the curves is less than 20% of the AUC of the estimated curve. The treatment LFA102 has a median sABC of only 0.153, indicating a good prediction. The worst predictions are in the treatment LGH447 with a median sABC of 0.867. Compared to the null model, the lasso reduced the sABC by a median decrease of 3.8%. This shows low predictive ability of the CNVs to predict tumor growth curves.

3.3.3 Identification of pathways associated with treatment efficacy and resistance

The TGI parameter values of k_d and k_r were regressed on CNVs grouped in pathways using the overlapping group lasso. The group lasso selected the pathways with predictive power for the 33 treatments where predictiveness was shown in the curve prediction step. Out of the 472 pathways from WikiPathways (Kutmon et al., 2015), 71

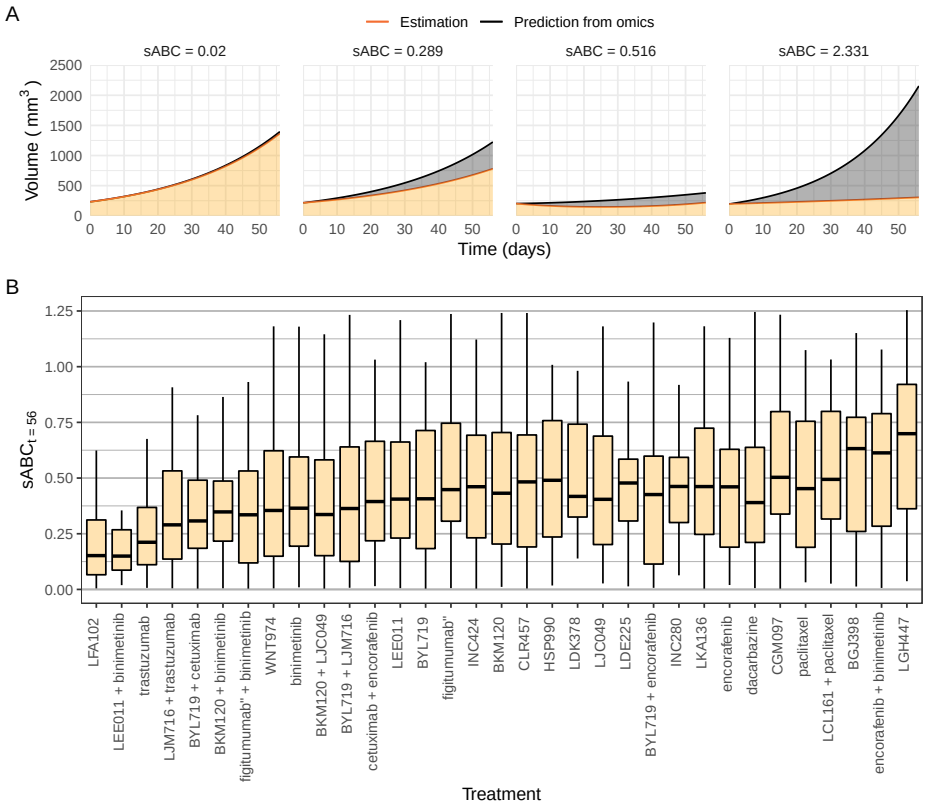

Figure 3.3: Predicted curves from the multivariate least absolute shrinkage and selection operator. A) Tumor growth curves visualized with the area under the estimated curve (orange) and between the estimated and predicted curves (grey) and the error (in scaled area between the predicted and the estimated curves [sABC]). From left to right show a very good prediction to a very poor prediction. B) The distributions of the individual patient-derived xenograft sABCs for the different treatments given by the interquartile range. Outliers are not included in the plot.

different pathways were selected for one or more of 19 different treatments, with a total of 118 detected pathway-treatment response correlations (Figure 3.4, Figure 3.5). The pathways were specifically correlated to either treatment efficacy or resistance development. More pathways were identified for k_d than k_r, due to smaller variation in k_r.

For paclitaxel, trastuzumab, encorafenib and figitumumab, the FDA approved drugs administered as monotherapy, we compared identified pathways with literature reports to evaluate their biological validity. We identified for 14 pathways for these four drugs, of which nine could be confirmed in literature (Table 3.1), where we confirm previously described mechanisms were detected through our method.

Figure 3.4: Selected pathways obtained by the group least absolute shrinkage and selection operator for the treatment efficacy (k_d = black), time- dependent resistance development (k_r = orange) or both (blue) over the different treatments. The distribution of pathways found for different treatments (top).

3.4 Discussion

In order to utilize high-dimensional omics data to further advance treatment response prediction and understanding, we developed a two-step approach combining a machine learning method with pharmacometric modeling.

We showed how CNVs can contribute to prediction of variability in tumor growth dynamics. This approach establishes a practical framework to enable personalized treatment selection or even dose optimization. Even though we have applied our approach to preclinical PDX data, TGI models have been widely used for modeling of clinical tumor size measurements to which our approach can be applied. Pharmacometric models including TGI models are typically based on ODE models, which is why we have chosen to formulate our model as ODEs and not using an analytical expression. Importantly, the use of a TGI model enables further integration with either clinical outcome prediction models (Claret et al., 2013) or it can be integrated with PK-PD models for TGI to refine dosing regimens to optimally suppress tumor growth. We expect this approach can also be implemented for the analysis of clinical tumor growth data.

In this study, we have set a cut-off of 56 days to evaluate the ability to back-predict tumor growth profiles; however, the predictions can also be extrapolated over a longer time-span, depending on the nature of available omics-data or specific disease or treatment characteristics. In terms of this sABC, the CNVs did however not show great improvement of predictive ability as compared to a null model. This was

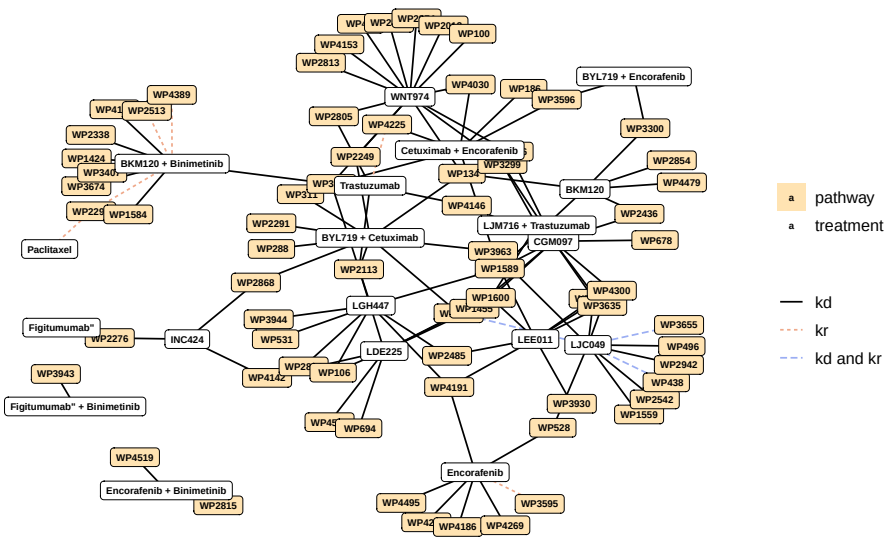

Figure 3.5: Overview of overlapping pathways between the different treatments. The nodes are the treatments (white background) and pathways (orange background) and the edges indicate which tumor growth inhibition parameter links the pathway to the treatment.

already visible in the large prediction errors on the tumor growth parameter values. The predictive ability was evaluated instead of the model fit in order to study more generalizable results. A large proportion of variance can often be explained by omics data, but the high-dimensional nature of the data makes it hard or impossible to distinguish between noise and structural differences.

To identify biological factors predictive for either treatment efficacy or resistance development we used a group lasso, grouping individual gene-associated CNVs to known biological pathways. We have used the Wikipathways ontology for grouping pathways, although other pathway databases can be used in a similar fashion. The pathway group lasso yields a set of pathways predictive of the outcomes treatment efficacy and time-dependent resistance development. Out of 14 identified pathways predictive of treatment efficacy and resistance development, nine pathways were confirmed by literature search. This is an indication of how omics pathway analysis for dynamic tumor growth responses could be a useful tool for validating pathway associations with factors responsible for treatment response, as well as discovering new correlations with pathways. Such a pathway-oriented approach has been previously proposed, but not in context with TGI or pharmacometric modeling (Silver et al., 2012).

In this study, we have used two versions of lasso regression for two distinct aims: variable selection and prediction. We selected the use of the lasso over other ML approaches due to its intrinsic property of variable selection.14 The selection for variables in high-dimensional data is not well accommodated in many algorithms, while the lasso inherently shrinks noise variables to zero. The lasso can achieve high sensitivity, but it can suffer from low specificity, this, however, is not considered as much of a problem in exploratory analyses.

The use of the group lasso allows for direct pathway selection based on omics data, which is computationally efficient and interpretable (Silver et al., 2012). The variable selection performance of the lasso has been investigated previously, and has been shown to perform competitively or comparatively better than other methods (Lenters et al., 2017; Hastie et al., 2017; Zheng & Liu, 2011).

The multivariate lasso was used to simultaneously predict the three model parameter values. A limitation of the multivariate lasso used in this study is that it does not take into account the dependence between the outcome variables, while the tumor growth model parameters are expected to be correlated. A second limitation was shown by the comparison between the predictions with and without adding k_r to the multivariate outcome. Prediction of one parameter can restrict the prediction of another parameter. We expect this problem can be overcome by better modeling of the joint and marginal distributions of the multivariate outcome.

The lasso has been previously implemented in pharmacometric nonlinear mixed effect models.16–18 These direct implementations have the advantage of informing the lasso directly within the longitudinal modeling. Models with a very high number of variables, however, become computationally hard. To our knowledge, these lasso implementations have not been successfully applied to very high-dimensional data, where the number of variables (p) was an order of magnitude larger than the number of observations (n), either due to convergence problems, or exploding computation

times. The two-step method is more dependent on the fit of the first model and the accuracy of the EBEs. Our method is more feasible in high-dimension, since the steps of the complex longitudinal model estimation and the high-dimensional predictors are separated.

The two-step approach can directly use other ML algorithms besides the lasso. Algorithms such as Random Forests and Gradient Boosting are able to capture non-linearity more easily, and can be used to improve model prediction accuracy. There is still a challenge in modeling multiple outcomes at the same time, such as the k_g, k_d and k_r in our study, but multivariate outcome modeling extensions have been made in in other high-dimensional methods, such as random forests (Segal & Xiao, 2011), which can be also used to predict tumor growth parameter values, as in the second step of our approach.

In summary, we demonstrated how combining machine learning and pharmacometric modeling can be used to gain pharmacological understanding of factors driving variation in treatment response, and to enable omics-based personalized treatment regimens.

Table 3.1: Pathway-treatment correlations found in literature. Scientific literature indicating previous findings on the pathways correlated to treatment efficacy and resistance, for the treatments paclitaxel, trastuzumab and encorafenib.

Treatment	Pathway	Response type	Literature	Relation
Paclitaxel	RalA downstream regulated genes (WP2290)	k_r	Ganapathy et al. (2016)	Paclitaxel is a mitotic inhibitor by stabilizing the microtubule and RalA has been previously shown to disrupt microtubule formation and inducing mitotic catastrophe.
Trastuzumab	Synthesis and degradation of ketone bodies (WP311)	k_d	Jobard et al. (2017)	Ketone production was shown to be increased with effective trastuzumab treatment.
	Macrophage markers (WP4146)	k_d	Shi et al. (2015)	Trastuzumab interacts with Fc$upgamma$ receptors on macrophages for the killing of HER2 cancer cells
	Pyrimidine metabolism and related diseases (WP4225)	k_d	Ghosh et al. (2009); Liu et al. (2019)	The pyrimidine metabolism pathway has been found in previous studies to correlate with drug response to Trastuzumab, based on pathway enrichment analysis in transcriptomics and metabolomics studies
	Caloric restriction and aging (WP4191)	k_d	Chappell et al. (2011)	There is a connection between Raf/MEK inhibitors and aging
	Somatroph axis (GH) and its relationship to dietary restriction and aging (WP4186)	k_d	Chappell et al. (2011)	There is a connection between Raf/MEK inhibitors and aging
Encorafenib	mir-124 predicted interactions with cell cycle and differentiation (WP3595)	k_r	Ross et al. (2018)	Resistance to Encorafenib has been shown to be correlated to cell cycle and differentiation
	Ethanol metabolism resulting in production of ROS by CYP2E1 (WP4269)	k_d	Friedlander and Cajulis (2019)	Ethanol metabolism resulting in production of ROS by CYP2E1 was found to have a connection to the development of melanoma, thus might be related to drug efficacy of encorafenib in melanoma treatment.
	IL-10 Anti-inflammatory Signaling Pathway (WP4495)	k_d	Sloane et al. (2017); Sumimoto et al. (2006)	IL-10 has been researched in the context of overexpression of Raf in cancer patients, showing that IL-10 is an immunosuppressive factor that is decreased by MEK inhibitors

References

Beal, S., & Sheiner, L. (1980, May). The NONMEM system. *The American Statistician*, *34*(2), 118. Retrieved from https://doi.org/10.2307%2F2684123 doi: 10.2307/2684123

Bender, B. C., Schindler, E., & Friberg, L. E. (2014, Dec). Population pharmacokinetic–pharmacodynamic modelling in oncology: a tool for predicting clinical response. *British Journal of Clinical Pharmacology*, *79*(1), 56–71. Retrieved from https://doi.org/10.1111%2Fbcp.12258 doi: 10.1111/bcp.12258

Bertrand, J., Comets, E., & Mentré, F. (2008, Nov). Comparison of model-based tests and selection strategies to detect genetic polymorphisms influencing pharmacokinetic parameters. *Journal of Biopharmaceutical Statistics*, *18*(6), 1084–1102. Retrieved from https://doi.org/10.1080%2F10543400802369012 doi: 10.1080/10543400802369012

Bertrand, J., Iorio, M. D., & Balding, D. J. (2015, May). Integrating dynamic mixed-effect modelling and penalized regression to explore genetic association with pharmacokinetics. *Pharmacogenetics and Genomics*, *25*(5), 231–238. Retrieved from https://doi.org/10.1097%2Ffpc.0000000000000127 doi: 10.1097/fpc.0000000000000127

Chadeau-Hyam, M., Campanella, G., Jombart, T., Bottolo, L., Portengen, L., Vineis, P., ... Vermeulen, R. C. (2013, Aug). Deciphering the complex: Methodological overview of statistical models to derive OMICS-based biomarkers. *Environmental and Molecular Mutagenesis*, *54*(7), 542–557. Retrieved from https://doi.org/10.1002%2Fem.21797 doi: 10.1002/em.21797

Chappell, W. H., Steelman, L. S., Long, J. M., Kempf, R. C., Abrams, S. L., Franklin, R. A., ... McCubrey, J. A. (2011, Mar). Ras/raf/MEK/ERK and PI3k/PTEN/akt/mTOR inhibitors: Rationale and importance to inhibiting these pathways in human health. *Oncotarget*, *2*(3), 135–164. Retrieved from https://doi.org/10.18632%2Foncotarget.240 doi: 10.18632/oncotarget.240

Chen, E. Y., Tan, C. M., Kou, Y., Duan, Q., Wang, Z., Meirelles, G. V., ... Ma'ayan, A. (2013, Apr). Enrichr: interactive and collaborative HTML5 gene list enrichment analysis tool. *BMC Bioinformatics*, *14*(1). Retrieved from https://doi.org/10.1186%2F1471-2105-14-128 doi: 10.1186/1471-2105-14-128

Claret, L., Girard, P., Hoff, P. M., Cutsem, E. V., Zuideveld, K. P., Jorga, K., ... Bruno, R. (2009, Sep). Model-based prediction of phase III overall survival in colorectal cancer on the basis of phase II tumor dynamics. *Journal of Clinical Oncology*, *27*(25), 4103–4108. Retrieved from https://doi.org/10.1200%2Fjco.2008.21.0807 doi: 10.1200/jco.2008.21.0807

Claret, L., Gupta, M., Han, K., Joshi, A., Sarapa, N., He, J., ... Bruno, R. (2013, Jun). Evaluation of tumor-size response metrics to predict overall survival in western and chinese patients with first-line metastatic colorectal cancer. *Journal of Clinical Oncology*, *31*(17), 2110–2114. Retrieved from https://doi.org/10.1200%2Fjco.2012.45.0973 doi: 10.1200/jco.2012.45.0973

Degenhardt, F., Seifert, S., & Szymczak, S. (2017, Oct). Evaluation of variable selection methods for random forests and omics data sets. *Briefings in Bioinformatics*, *20*(2), 492–503. Retrieved from https://doi.org/10.1093%2Fbib%2Fbbx124 doi: 10.1093/bib/bbx124

Eisenhauer, E., Therasse, P., Bogaerts, J., Schwartz, L., Sargent, D., Ford, R., ... Verweij, J. (2009, Jan). New response evaluation criteria in solid tumours: Revised RECIST guideline (version 1.1). *European Journal of Cancer*, *45*(2), 228–247. Retrieved from https://doi.org/10.1016%2Fj.ejca.2008.10.026 doi: 10.1016/j.ejca.2008.10.026

Friedlander, P., & Cajulis, C. B. (2019, Aug). *Melanoma*. Wiley. Retrieved from https://doi.org/10.1002%2F9781119189596.ch18 doi: 10.1002/9781119189596.ch18

Ganapathy, S., Fagman, J. B., Shen, L., Yu, T., Zhou, X., Dai, W., ... Chen, C. (2016, Oct). Ral a, via activating the mitotic checkpoint, sensitizes cells lacking a functional nf1 to apoptosis in the absence of protein kinase c. *Oncotarget*, *7*(51), 84326–84337. Retrieved from https://doi.org/10.18632%2Foncotarget.12607 doi: 10.18632/oncotarget.12607

Gao, H., Korn, J. M., Ferretti, S., Monahan, J. E., Wang, Y., Singh, M., ... Sellers, W. R. (2015, Oct). High-throughput screening using patient-derived tumor xenografts to predict clinical trial drug response. *Nature Medicine*, *21*(11), 1318–1325. Retrieved from https://doi.org/10.1038%2Fnm.3954 doi: 10.1038/nm.3954

Ghosh, R., Narasanna, A., Gonazalez-Angulo, A., Mills, G., & Arteaga, C. (2009, Dec). Differential signaling by ErbB receptor (HER) dimers: Implications for response to anti-HER2 therapies in breast cancer. *Cancer Research*, *69*(24_Supplement), 705–705. Retrieved from https://doi.org/10.1158%2F0008-5472.sabcs-09-705 doi: 10.1158/0008-5472.sabcs-09-705

Haem, E., Harling, K., Ayatollahi, S. M. T., Zare, N., & Karlsson, M. O. (2017, Jan). Adjusted adaptive lasso for covariate model-building in nonlinear mixed-effect pharmacokinetic models. *Journal of Pharmacokinetics and Pharmacodynamics*, *44*(1), 55–66. Retrieved from https://doi.org/10.1007%2Fs10928-017-9504-6 doi: 10.1007/s10928-017-9504-6

Hastie, T., Tibshirani, R., & Tibshirani, R. J. (2017, Jul). Extended Comparisons of Best Subset Selection, Forward Stepwise Selection, and the Lasso. *arXiv*, 1–19. Retrieved from http://arxiv.org/abs/1707.08692

Hoerl, A. E., & Kennard, R. W. (1970, Feb). Ridge regression: Biased estimation for nonorthogonal problems. *Technometrics*, *12*(1), 55–67. Retrieved from https://doi.org/10.1080%2F00401706.1970.10488634 doi: 10.1080/00401706.1970.10488634

Jacob, L., Obozinski, G., & Vert, J.-P. (2009). Group lasso with overlap and graph lasso. In *Proceedings of the 26th annual international conference on machine learning - ICML '09*. ACM Press. Retrieved from https://doi.org/10.1145%2F1553374.1553431 doi: 10.1145/1553374.1553431

Jobard, E., Trédan, O., Bachelot, T., Vigneron, A. M., Aït-Oukhatar, C. M., Arnedos, M., ... Elena-Herrmann, B. (2017, Jun). Longitudinal serum metabolomics evaluation of trastuzumab and everolimus combination as pre-operative treatment for HER-2 positive breast cancer patients. *Oncotarget*, *8*(48), 83570–83584. Retrieved from https://doi.org/10.18632%2Foncotarget.18784 doi: 10.18632/oncotarget.18784

Kuleshov, M. V., Jones, M. R., Rouillard, A. D., Fernandez, N. F., Duan, Q., Wang, Z., ... Ma'ayan, A. (2016, May). Enrichr: a comprehensive gene set enrichment analysis web server 2016 update. *Nucleic Acids Research*, *44*(W1), W90–W97. Retrieved from https://doi.org/10.1093%2Fnar%2Fgkw377 doi: 10.1093/nar/gkw377

Kutmon, M., Riutta, A., Nunes, N., Hanspers, K., Willighagen, E. L., Bohler, A., ... Pico, A. R. (2015, Oct). WikiPathways: capturing the full diversity of pathway knowledge. *Nucleic Acids Research*, *44*(D1), D488–D494. Retrieved from https://doi.org/10.1093%2Fnar%2Fgkv1024 doi: 10.1093/nar/gkv1024

Lathrop, K., & Kaklamani, V. (2018, Dec). The response evaluation criteria in solid tumors (RECIST). In *Predictive biomarkers in oncology* (pp. 501–511). Springer International Publishing. Retrieved from https://doi.org/10.1007%2F978-3-319-95228-4_46 doi: 10.1007/978-3-319-95228-4_46

Lenters, V., Vermeulen, R., & Portengen, L. (2017, Sep). Performance of variable selection methods for assessing the health effects of correlated exposures in case–control studies. *Occupational and Environmental Medicine*, *75*(7), 522–529. Retrieved from https://doi.org/10.1136%2Foemed-2016-104231 doi: 10.1136/oemed-2016-104231

Liu, W., Wang, Q., & Chang, J. (2019). Global metabolomic profiling of trastuzumab resistant gastric cancer cells reveals major metabolic pathways and metabolic signatures based on UHPLC-q exactive-MS/MS. *RSC Advances*, *9*(70), 41192–41208. Retrieved from https://doi.org/10.1039%2Fc9ra06607a doi: 10.1039/c9ra06607a

Nguyen, T. H. T., Mouksassi, M.-S., Holford, N., Al-Huniti, N., Freedman, I., Hooker, A. C., ... and, F. M. (2017, Feb). Model evaluation of continuous data pharmacometric models: Metrics and graphics. *CPT: Pharmacometrics & Systems Pharmacology*, *6*(2), 87–109. Retrieved from https://doi.org/10.1002%2Fpsp4.12161 doi: 10.1002/psp4.12161

Nicolò, C., Périer, C., Prague, M., Bellera, C., MacGrogan, G., Saut, O., & Benzekry, S. (2020, Nov). Machine learning and mechanistic modeling for prediction of metastatic relapse in early-stage breast cancer. *JCO Clinical Cancer Informatics*(4), 259–274. Retrieved from https://doi.org/10.1200%2Fcci.19.00133 doi: 10.1200/cci.19.00133

R Core Team. (2020). R: A Language and Environment for Statistical Computing [Computer software manual]. Vienna, Austria. Retrieved from https://www.r-project.org/

Ribba, B., Holford, N., Magni, P., Trocóniz, I., Gueorguieva, I., Girard, P., ... Friberg, L. (2014, May). A review of mixed-effects models of tumor growth and effects of anticancer drug treatment used in population analysis. *CPT: Pharmacometrics & Systems Pharmacology*, *3*(5), 113. Retrieved from https://doi.org/10.1038%2Fpsp.2014.12 doi: 10.1038/psp.2014.12

Ribbing, J., Nyberg, J., Caster, O., & Jonsson, E. N. (2007, May). The lasso—a novel method for predictive covariate model building in nonlinear mixed effects models. *Journal of Pharmacokinetics and Pharmacodynamics*, *34*(4), 485–517. Retrieved from https://doi.org/10.1007%2Fs10928-007-9057-1 doi: 10.1007/s10928-007-9057-1

Rodriguez-Brenes, I. A., Komarova, N. L., & Wodarz, D. (2013, Oct). Tumor growth dynamics: insights into evolutionary processes. *Trends in Ecology & Evolution*, *28*(10), 597–604. Retrieved from https://doi.org/10.1016%2Fj.tree.2013.05.020 doi: 10.1016/j.tree.2013.05.020

Ross, K. C., Chin, K. F., Kim, D., Marion, C. D., Yen, T. J., & Bhattacharjee, V. (2018, Jan). Methotrexate sensitizes drug-resistant metastatic melanoma cells to braf v600e inhibitors dabrafenib and encorafenib. *Oncotarget*, *9*(17), 13324–13336. Retrieved from https://doi.org/10.18632%2Foncotarget.24341 doi: 10.18632/oncotarget.24341

Segal, M., & Xiao, Y. (2011, Jan). Multivariate random forests. *WIREs Data Mining and Knowledge Discovery*, *1*(1), 80–87. Retrieved from https://doi.org/10.1002%2Fwidm.12 doi: 10.1002/widm.12

Sheiner, L. B., Rosenberg, B., & Melmon, K. L. (1972, Oct). Modelling of individual pharmacokinetics for computer-aided drug dosage. *Computers and Biomedical Research*, *5*(5), 441–459. Retrieved from https://doi.org/10.1016%2F0010-4809%2872%2990051-1 doi: 10.1016/0010-4809(72)90051-1

Shi, Y., Fan, X., Deng, H., Brezski, R. J., Rycyzyn, M., Jordan, R. E., ... An, Z. (2015, Mar). Trastuzumab triggers phagocytic killing of high HER2 cancer cells in vitro and in vivo by interaction with fcgamma receptors on macrophages. *The Journal of Immunology*, *194*(9), 4379–4386. Retrieved from https://doi.org/10.4049%2Fjimmunol.1402891 doi: 10.4049/jimmunol.1402891

Shlien, A., & Malkin, D. (2009). Copy number variations and cancer. *Genome Medicine*, *1*(6), 62. Retrieved from https://doi.org/10.1186%2Fgm62 doi: 10.1186/gm62

Silver, M., Montana, G., & In, A. D. N. (2012, Jan). Fast identification of biological pathways associated with a quantitative trait using group lasso with overlaps. *Statistical Applications in Genetics and Molecular Biology*, *11*(1), 1–43. Retrieved from https://doi.org/10.2202%2F1544-6115.1755 doi: 10.2202/1544-6115.1755

Simon, N., Friedman, J., & Hastie, T. (2013, Nov). A Blockwise Descent Algorithm for Group-penalized Multiresponse and Multinomial Regression. *arXiv*. Retrieved from http://arxiv.org/abs/1311.6529 doi: 10.48550/arXiv.1311.6529

Sloane, R. A. S., Gopalakrishnan, V., Reddy, S. M., Zhang, X., Reuben, A., & Wargo, J. A. (2017, May). Interaction of molecular alterations with immune response in melanoma. *Cancer*, *123*(S11), 2130–2142. Retrieved from https://doi.org/10.1002%2Fcncr.30681 doi: 10.1002/cncr.30681

Sumimoto, H., Imabayashi, F., Iwata, T., & Kawakami, Y. (2006, Jun). The BRAF–MAPK signaling pathway is essential for cancer-immune evasion in human melanoma cells. *Journal of Experimental Medicine*, *203*(7), 1651–1656. Retrieved from https://doi.org/10.1084%2Fjem.20051848 doi: 10.1084/jem.20051848

Tibshirani, R. (1996, Jan). Regression shrinkage and selection via the lasso. *Journal of the Royal Statistical Society: Series B (Methodological)*, *58*(1), 267–288. Retrieved from https://doi.org/10.1111%2Fj.2517-6161.1996.tb02080.x doi: 10.1111/j.2517-6161.1996.tb02080.x

van Hasselt, J., Gupta, A., Hussein, Z., Beijnen, J., Schellens, J., & Huitema, A. (2015a, Jun). Disease progression/clinical outcome model for castration-resistant prostate cancer in patients treated with eribulin. *CPT: Pharmacometrics & Systems Pharmacology*, *4*(7), 386–395. Retrieved from https://doi.org/10.1002%2Fpsp4.49 doi: 10.1002/psp4.49

van Hasselt, J., Gupta, A., Hussein, Z., Beijnen, J., Schellens, J., & Huitema, A. (2015b, Jun). Integrated simulation framework for toxicity, dose intensity, disease progression, and cost effectiveness for castration-resistant prostate cancer treatment with eribulin. *CPT: Pharmacometrics & Systems Pharmacology*, *4*(7), 374–385. Retrieved from https://doi.org/10.1002%2Fpsp4.48 doi: 10.1002/psp4.48

Xie, G., Dong, C., Kong, Y., Zhong, J., Li, M., & Wang, K. (2019, Mar). Group lasso regularized deep learning for cancer prognosis from multi-omics and clinical features. *Genes*, *10*(3), 240. Retrieved from https://doi.org/10.3390%2Fgenes10030240 doi: 10.3390/genes10030240

Yuan, M., & Lin, Y. (2006, Feb). Model selection and estimation in regression with grouped variables. *Journal of the Royal Statistical Society: Series B (Statistical Methodology)*, *68*(1), 49–67. Retrieved from https://doi.org/10.1111%2Fj.1467-9868.2005.00532.x doi: 10.1111/j.1467-9868.2005.00532.x

Zheng, S., & Liu, W. (2011, Nov). An experimental comparison of gene selection by lasso and dantzig selector for cancer classification. *Computers in Biology and Medicine*, *41*(11), 1033–1040. Retrieved from https://doi.org/10.1016%2Fj.compbiomed.2011.08.011 doi: 10.1016/j.compbiomed.2011.08.011

Supplementary material

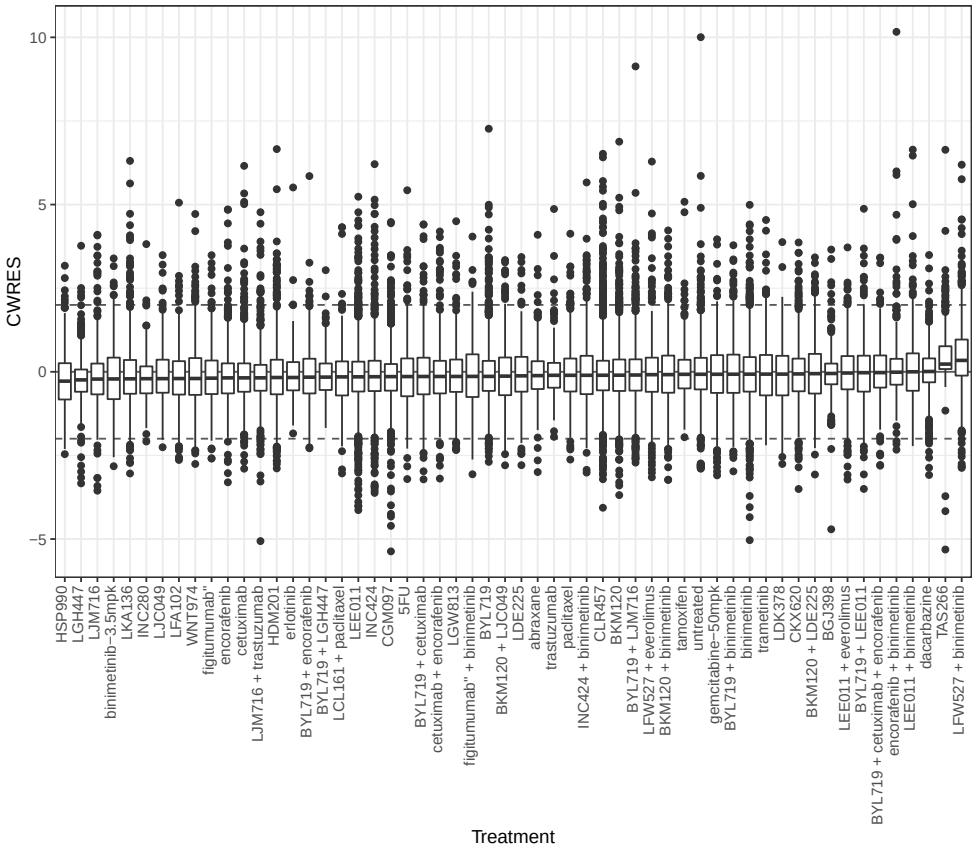

Figure S3.1: The conditional weighted residuals over the different treatments.

Table S3.1: Number of observations for every treatment, that were used in the second step of the analysis for the prediction of growth curves and the pathway selection.

Treatment	Number of PDXs
5FU	41
abraxane	33
BGJ398	62
binimetinib	166
binimetinib-3.5mpk	34
BKM120	168
BKM120 + binimetinib	56
BKM120 + LDE225	31
BKM120 + LJC049	39
BYL719	138
BYL719 + binimetinib	40
BYL719 + cetuximab	39
BYL719 + cetuximab + encorafenib	40
BYL719 + encorafenib	39
BYL719 + LEE011	36
BYL719 + LGH447	24
BYL719 + LJM716	133
cetuximab	64
cetuximab + encorafenib	39
CGM097	129
CKX620	64
CLR457	156
dacarbazine	30
encorafenib	72
encorafenib + binimetinib	32
erlotinib	22
figitumumab”	36
figitumumab” + binimetinib	35
gemcitabine-50mpk	32
HDM201	134
HSP990	22
INC280	23
INC424	69
INC424 + binimetinib	32
LCL161 + paclitaxel	23
LDE225	30
LDK378	31
LEE011	166
LEE011 + binimetinib	17
LEE011 + everolimus	37
LFA102	37
LFW527 + binimetinib	44
LFW527 + everolimus	29
LGH447	25
LGW813	32
LJC049	39
LJM716	38
LJM716 + trastuzumab	37
LKA136	111
paclitaxel	61
tamoxifen	38
TAS266	32
trametinib	34
trastuzumab	37
untreated	171
WNT974	65

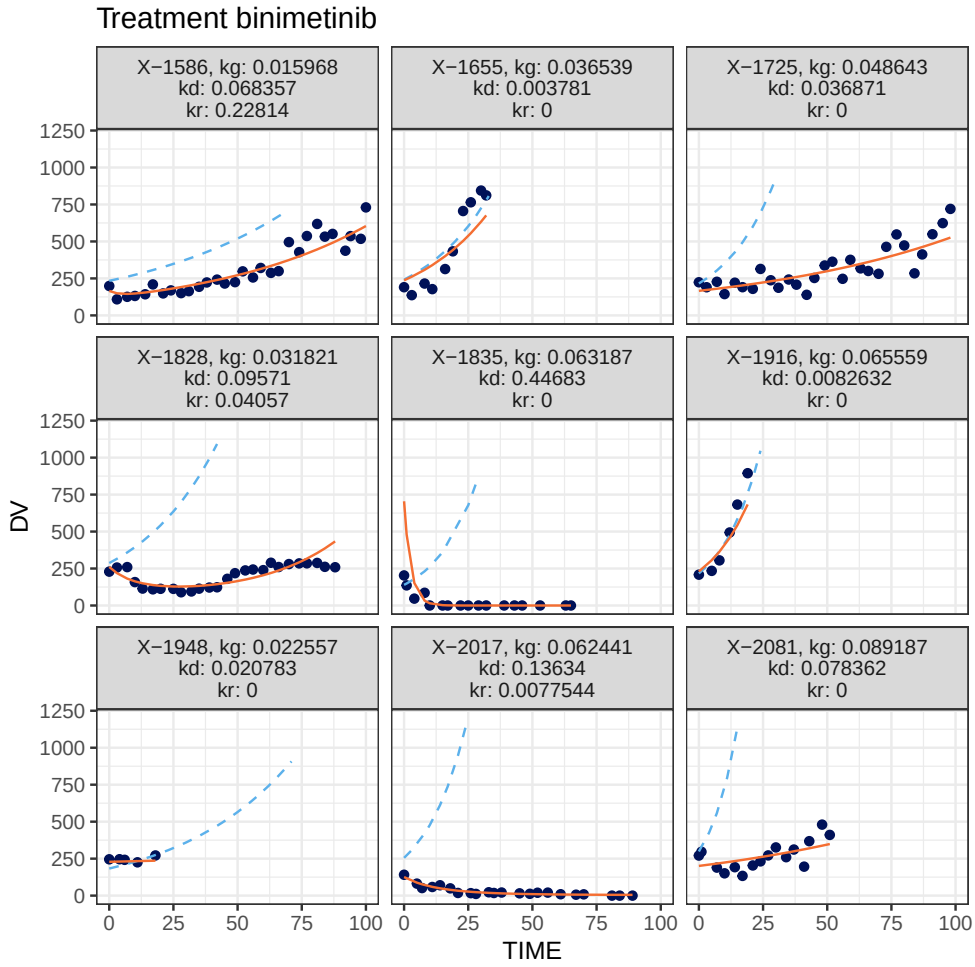

Figure S3.2: Set of figures with the non–linear mixed effect model fits for a subset of PDXs. Within every treatment, the volume (DV) is plotted against time (TIME) for every PDX. The modeled natural growth curves are shown (blue dashed line) and the model (red solid line) fit to the observed values (dark blue points). Tumor growth curves from treatment TAS266 show a bad model fit. Figures with model fits for all PDXs can be found online:

https://ascpt.onlinelibrary.wiley.com/action/downloadSupplement?doi=10.1002%2Fpsp4.12603&file=psp412603-sup-0002-FigS2.pdf

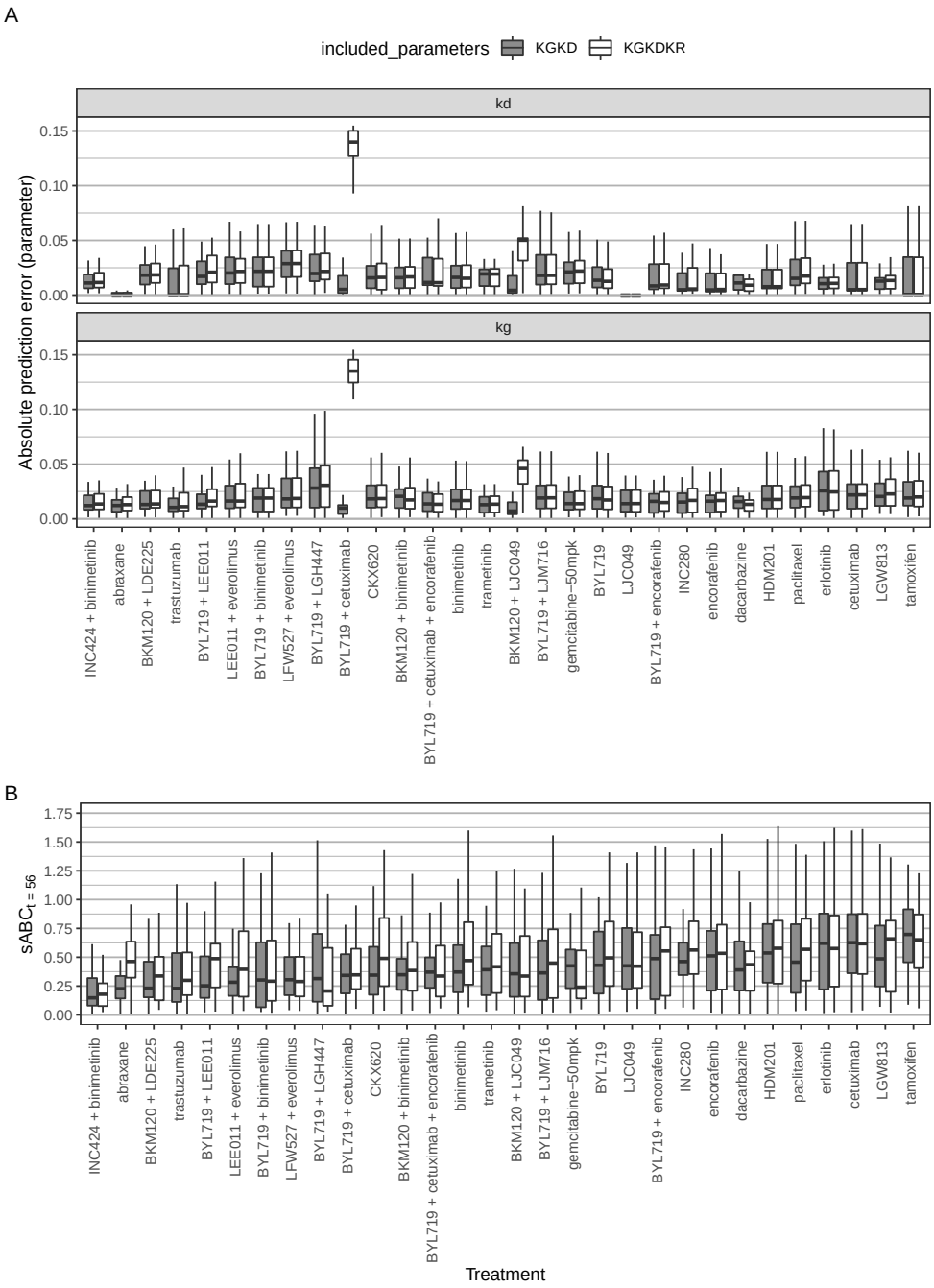

Figure S3.3: The prediction errors for the two models with (white) and without (grey) inclusion of k_r in the multivariate lasso for all treatments where the k_r was estimated non-zero in the non-linear mixed effect estimation. A) the absolute prediction error of the parameter values. B) the sABC for the same treatments. Both the prediction errors and the sABC are generally higher for the lasso without inclusion of k_r.